ELSEVIER

Contents lists available at ScienceDirect

Alexandria Engineering Journal

journal homepage: www.elsevier.com/locate/aej





Computational study of the combined impacts of variable density of the hydrosphere and thermal jump in atmosphere on climate change

Rabia Iqbal^a, Muhammad Ashraf^a, Ghulam Rasool^{b,*}, Ali Saeed Alqahtani^c, Muhammad Yousaf Malik^c, Ali J. Chamkha^d

- ^a Department of Mathematics, Faculty of Science, University of Sargodha, Sargodha 10400, Pakistan
- Department of Mechanical Engineering, College of Engineering, Prince Mohammad Bin Fahd University, P. O. Box, 1664, Al-Khobar 31952, Saudi Arabia
- Department of Mathematics, College of Sciences, King Khalid University, Abha 61413, Saudi Arabia
- ^d Faculty of Engineering, Kuwait College of Science and Technology, Doha District, 35004, Kuwait

ARTICLE INFO

Keywords: Natural convection Concentric sphere Atmosphere Hydrosphere Trans-boundary Thermal jump Variable density Finite difference method

ABSTRACT

This current work highlights the impact of variable density of hydrosphere and atmosphere on climate change by introducing thermal jump effects in atmosphere region. For this purpose, a mathematical model is developed in two regions, the atmosphere region and the hydrosphere region in terms of a spherical coordinate system. In this natural phenomenon solar energy is received by the earth surface and shifted towards hydrosphere and atmosphere. The hydrosphere absorbs more energy as compare to atmosphere, keeping in view this natural phenomenon, these two regions are assumed at high temperature difference and there is a trans-boundary because of this large difference. The phenomenon of convective heat transfer between two regions influenced by the thermal jump condition included in the atmosphere. Changes in density affect how this heat is transported to the atmosphere. Thermal jumps in the atmosphere alter the radiative and convective heat exchange between the surface and the upper atmosphere. The effects of significant parameters that are pertinent to hydrosphere and atmosphere are observed and examined to establish climate predictions. In order to integrate the partial differential equations, the finite difference method is used and then the obtained system of algebraic equations is solved using Gaussian elimination method. It is found that velocity profile decreases and temperature distribution increases with increasing density variation parameter in hydrosphere region at $\gamma = 1.5$ radian. The temperature profile and velocity profile has maximum and minimum values, respectively for $\beta_H=1.0$ at position $\gamma=1.5$ radian, whereas thermal distribution is minimum for $\beta_H=0.02$ and velocity distribution is maximum for $\beta_H=0.08$ at $\gamma=1.5$ radian. Additionally it is noted that the velocity profile and thermal profile with increasing values of S_T , the velocity profile and temperature profile is increased. Consequently both have maximum magnitudes on $S_T = 0.07$ at the position $\gamma^* = 3.0$. It is further observed that the interplay between the variable density of the hydrosphere and thermal inversion in the atmosphere influences the climate in diverse ways, particularly during thermal interactions between these two systems. Variations in hydrospheric density can significantly affect the development and intensity of weather events like hurricanes and monsoons. Moreover, atmospheric temperature inversions caused by thermal jumps can lead to the formation of oceanic layer fog.

1. Introduction

In the context of hydrosphere and atmosphere natural convection is driven by buoyancy forces that is the consequence of temperature differences. Hydrosphere has high heat capacity than atmosphere that allows it to absorb and store significant amount of heat emitted from the earth as compare to atmosphere. Hydrosphere absorbs heat during the

day and it releases heat at night to moderate coastal and global temperatures. The density of hydrosphere decreases with increase in temperature, resulting in the formation of distinct thermal layers, the warmer less dense surface layer and the cooler denser deep layer. This layering due to density differences affects heat distribution and ocean mixing processes. An increased stratification can boost the hydrosphere's aptitude to trap heat, contributing to longer-term warming trends. The warmer surface of sea transfers heat to lower atmosphere

E-mail addresses: rabia.muhammad@uos.edu.pk (R. Iqbal), muhammad.ashraf@uos.edu.pk (M. Ashraf), grasool@pmu.edu.sa (G. Rasool), alqahtani@kku.edu.sa (A.S. Alqahtani), mmuhammadramzan@kku.edu.sa (M.Y. Malik), achamkha@yahoo.com (A.J. Chamkha).

 $^{^{\}ast}$ Corresponding author.

Nomenclature		T	Hydrosphere Temperature (K)		
		T^*	Atmosphere Temperature (K)		
Pr_H	Prandtl number for Hydrosphere	T_{∞}	Temperature far away the atmospheric surface		
Pr_A	Prandtl number for Atmosphere	T_w	Hydrosphere Surface temperature (K)		
Gr_H	Grashof number for hydrosphere	T_0	Atmosphere Surface temperature (K)		
Gr_A	Grashof number for Atmosphere	ϕ	Non-dimensional temperature of hydrosphere		
C_p	Hydrosphere Specific heat $(Jkg^{-1}K^{-1})$	$oldsymbol{\phi}^*$	Non-dimensional temperature of atmosphere		
C_p^*	Atmospheric Specific heat $(Jkg^{-1}K^{-1})$	k	Hydrosphere Thermal conductivity		
-	Hydrosphere Velocities along r, θ -direction (ms^{-1})	$oldsymbol{k}^*$	Atmosphere Thermal conductivity		
., 0	Atmosphere Velocities along r , θ *-direction (ms^{-1})	β	Hydrosphere Thermal expansion coefficient (K^{-1})		
u_r^*, u_θ^*	1	υ	Hydrosphere Kinematic viscosity (m^2s^{-1})		
g	Hydrosphere Gravitational acceleration (ms^{-2})	μ	Hydrosphere Dynamic viscosity (Nsm ⁻²)		
g *	Atmosphere Gravitational acceleration (ms^{-2})	ρ	Hydrosphere density		
$\widehat{u}_r, \widehat{u}_{ heta}$	Hydrosphere Non-dimensional Velocities along r, θ	$oldsymbol{eta}^*$	Atmosphere Thermal expansion coefficient (K^{-1})		
	-direction	μ*	Atmosphere Dynamic viscosity (Nsm ⁻²)		
$\widehat{u}_r^*, \widehat{u}_{\theta}^*$	Atmosphere Non-dimensional Velocities along r , θ	, *ט	Atmosphere Kinematic viscosity (m^2s^{-1})		
	-direction	$ ho^*$	Atmospheric density		
\widehat{r}	Non-dimensional distance normal to the surface	$ ho_{\infty}^{*}$	reference density		
$\widehat{ heta}$	Non-dimensional distance along the surface	γ	location representative for hydrosphere region.		
$\widehat{\pmb{r}}^*$	Non-dimensional distance normal to the surface	γ*	location representative for atmosphere region.		
$\widehat{ heta}^*$	Non-dimensional distance along the surface	•			

which drives the monsoon systems and affecting rainfall patterns in sea region. The temperature-dependent density of seawater acutely influences the thermal interactions between the hydrosphere and the atmosphere in sea regions as it can affect the formation and intensity of weather phenomena. When in this thermal interaction a thermal jump condition appears in atmosphere the rate of energy exchange is not adequate to maintain thermal equilibrium. The warm, moist air from the ocean surface is stuck below the thermal jump, leading to increased humidity resulting in fog or low-lying clouds but may stop the formation of higher-altitude clouds and precipitation. Constant temperature inversion can lead to increase in the ocean's surface layer, possibly disturbing ocean circulation patterns and contributing to regional climate glitches. This research aims to build a robust framework for understanding the temperature dependent density effects for hydrosphere and atmosphere thermal interaction in the presence of thermal jump condition in atmosphere regions by conducting a comprehensive review of existing literature. Keeping in view the above understanding, we highlight the work of some authors to establish the mathematical model of proposed problem.

Natural convection grows one of the major topics of research in the last two centuries. But flow and heat transfer between multiphase flow in curvilinear geometries are extensively seeking attention because of wide range of applications occur in industrial and technological and Climate fields. Koh et al. [1] observed two-phase flow phenomena in a laminar film compression, which occurs as a result of the vapor's convincing movements. For Pr> 10, it is discovered that the impact on heat transfer at the liquid-vapor interface is minimal. For the liquid metal range, interfacial caused the significant decreases in heat transmission. Banks in [2] investigated the boundary layer flow engendered by a rotating sphere, using the series expansion numerically. Mack & Hardee [3] determined the solution for a fluid that has stable axisymmetric convection and is bounded in the middle of isothermal concentric circles. Heat transfer rates, temperature profiles, Rayleigh numbers, and Prandtl numbers for natural convection between isothermal concentric spheres were reported by Scanlan et al. [4] for various gap radius ratios. By preserving the proper temperature differential between two concentric spherical surfaces, Caltagirone et al. [5] found that unicellular flow has a greater propensity to act than the multicellular regime. Hsin-Sen & Tzong-Shing [6] used a finite difference method to handle the problem of transient heat transport by natural convection within two concentric isothermal spheres. It was shown that the ratio of radius to Rayleigh number has a substantial effect on the temperature and flow fields. Webster's [7] study indicates that determining the size of the primary atmospheric circulation patterns depends critically on the thermodynamics of marine and atmospheric systems during hydrological cycles. Verzicco & Orlandi [8] provided a second-order finite-difference method for the flow that is incompressible in cylindrical coordinates. Khodadadi & Zhang [9] propose a computational investigation on the impact of buoyancy-driven convection on melting materials inside spherical containers. The hydrodynamic and thermal properties of the steady forced convective boundary layer flow across a porous plate embedded in a Darcy porous medium with slip at the boundary were obtained numerically by Bhattacharyya et al. [10]. Sheremet [11] discovered that an increase in Rayleigh number causes asymmetric thermo-hydrodynamic to occur in a sphere that is heated at the bottom and cooled at the top. Ibrahim & Shankar [12] examined the effects of a magnetic field, a slip boundary condition, and thermal radiation on boundary layer flow and heat transfer over a permeable stretched sheet. A model of heat transfer and fluid flow during the melting of a phase-change material inside a closed, uniformly heated spherical shell was developed by Archibold et al. [13]. A continuously moving vertical plate with mixed convection flow with slip and convective heat transfer was studied by Singh & Makinde [14] in the presence of a uniform free stream. An incompressible tangent Hyperbolic non-Newtonian fluid's nonlinear free convection boundary layer flow and heat transfer from a vertical porous plate with velocity slip and thermal jump impacts were presented by Ramachandra et al. [15]. In Siddiga et al. [16] model, the fluid density is assumed to be an exponential function of temperature and it deals with the two-dimensional natural convection flow of a radiating fluid over a horizontal circular disk. A mathematical model was constructed by Khan et al. [17] to investigate the magneto-hydrodynamic (MHD) flow caused by a nonlinear stretching cylinder in the presence of velocity and thermal slip of a viscous fluid. In order to describe transient natural convection using a non-Boussinesq approximation for changeable characteristics, huge temperature variations, and varied Rayleigh numbers, Armengol et al. [18] obtained a numerical solution. The numerical solutions for the non-Newtonian fluid's unsteady flow and heat transfer with slip effects were reported by Hamid et al. [19]. The impact of surface temperature oscillation and free-stream velocity on unstable mixed convection was

examined by Ullah et al. [20] using the dimensionless MHD boundary-layer equations. In their study, Ashraf et al. [21] examined the oscillatory mixed convection flow of an electrically conducting fluid along a horizontal circular cylinder that is non-conducting. The flow was subjected to variable density, which is considered to vary exponentially with temperature. Ahmad et al. [22] studied the free convective boundary layer flow of a viscous incompressible fluid with temperature-dependent viscosity and thermal conductivity in the setting of an exothermic catalytic chemical process that proceeds along a curved path. Ashraf et al. [23] examines the effects of viscous dissipation and thermophoretic motion on a two-dimensional fluid moving at various positions on a sphere while taking slip flow into consideration. Ullah et al. [24] used numerical observation to measure the amplitude of time-dependent skin friction, heat transfer, and current density at appropriate non-conducting cylinder positions. By increasing the various amounts of relevant physical parameters, it was observed that the maximum amplitude of all the amounts is at position $\alpha = \pi/2$. The effects of solar radiation on Casson fluid flow and heat transfer over an exponentially stretched sheet were studied by Abbas et al. [25] while taking into account the role of temperature-dependent thermal conductivity. Thermal and velocity slips' effects on the mixed convective flow of an electrically conducting fluid along a surface that is symmetrically heated and magnetized were examined by Alharbi et al. [26]. Sridhar and Muthtamilselvan [27] conducted a study on Jeffrey fluid stability analysis in microbial systems of anisotropic porous media with emergent chemical gradients. With Boussinesq estimation and the Jeffrey-Darcy type, the analysis is carried out. Regardless of the bioconvection Lewis number Le, the traditional thermal Rayleigh Darcy number is determined as a comprehensive function of multiple parameters. Saraswathy et al. [28] investigated the rate of heat transfer for micropolar fluid in a channel flow. The Cattaneo-Christov heat flux design is used in energy systems regardless of formal Fourier's law. The heat transmission of two-phase concurrent flow through a vertical, cylindrical, homogenous porous material was examined by Abdelaziz et al. [29]. Their focus is on a general form of the Darcy flow model for each phase and the system energy equation. Air/water downward flow, spherical beads, a ratio of particle diameter to pipe radius D = 0.412, porosity $\phi = 0.396,~0.01 \le Re \le 500,~water~to~air~volume~ratio$ $0 \le W/A \le \infty$, and saturation ratio $0 \le S_1 \le 1$ are all used to experimentally validate the numerical results. By developing the suggested problem mathematical model based on three regions, the source region (in terms of rectangular coordinates), the plume region (in terms of cylindrical coordinates), and the atmospheric region (in terms of spherical coordinates), Nadeem et al. [30] examined the effects of fossil fuel thermophoretic convective heat transfer on climate change with variable viscosity and thermal conductivity.

The present research investiates the effects of variable density of hydrosphere and atmosphere with thermal jump condition on thermal convection in sea region in terms of climate change. Two dimensional axi-symmetric spherical mathematical model has been established. By employing primitive variable formulation, the governing equations are transformed into suitable system of equations and then solved numerically with the aid of finite difference numerical technique in connection with Gaussian elimination technique. The physical situation is comprehended graphically through velocity and temperature profiles along with heat transfer mechanism in both regions. The novelty of this work lies in its integrative approach, addressing underexplored interactions between atmospheric and oceanic systems with computational modelling. The density of the hydrosphere is affected by temperature, salinity, and pressure. These variations impact global circulation patterns, ocean heat transport, and climate regulation. The concept of "thermal jumps" refers to abrupt temperature changes across atmospheric layers, often tied to phenomena like jet streams or large-scale circulation changes. Investigating how these thermal gradients interact with hydrosphere dynamics is a fresh area of research. Computational models that simulate these density gradients can uncover novel feedback mechanisms in

the Earth's climate system. Such models could improve understanding of extreme weather events, long-term climate shifts, and tipping points.

2. Mathematical formulation

This study examines the natural convection heat transfers from the hydrosphere to the atmosphere, both have different physical features. It is assumed that the hydrosphere's density varies and that in atmospheric phase thermal jump boundary condition exists. The coordinate system under consideration is illustrated in Fig. 1, comprising of two concentric spheres. The inner sphere, situated above the hydrosphere, signifies the hydrosphere's surface, which is connected to the outer sphere, which represents the atmosphere. It is considered that there is an adjacent layer between the hydrosphere and atmosphere due to a temperature difference, evaporation at the interface is neglected, and the boundary separating the two is a soft boundary. Since Fig. 1's geometry is axisymmetric, growing θ (distance along the flow) and r (normal distance) are related to the velocity components (u_r, u_θ) . The temperatures of the hydrosphere and atmosphere are represented by $T = T(r, \theta)$ and $T^* = T^*(r^*, \theta^*)$, respectively, with $r = \delta$ signifying the interface between the two phases. We have selected the coordinates (r^*, θ^*) for the atmosphere, where θ moves around the interface's circumference, r^* measures its normal, and (u_r^*, u_θ^*) are the velocity components that correspond to (r^*, θ^*) . Furthermore, the system of governing equations that follows [2] and [11] is based on the assumption that changes in all physical quantities occur in radial directions.

Hydrosphere phase

$$\frac{\partial u_r}{\partial r} + \frac{1}{a sin \theta} \frac{\partial sin \theta u_{\theta}}{\partial \theta} = 0, \tag{1}$$

$$u_{r}\frac{\partial u_{\theta}}{\partial r} + \frac{u_{\theta}}{a}\frac{\partial u_{\theta}}{\partial \theta} = \mu \frac{\partial}{\partial r} \left(\frac{1}{\rho}\frac{\partial u_{\theta}}{\partial r}\right) \pm g\beta(T - T^{*})\cos\gamma, \tag{2}$$

$$u_r \frac{\partial T}{\partial r} + \frac{u_\theta}{a} \frac{\partial T}{\partial \theta} = \frac{k}{C_p} \frac{\partial}{\partial r} \left(\frac{1}{\rho} \frac{\partial T}{\partial r} \right). \tag{3}$$

Atmosphere phase

$$\frac{-\partial u_r^*}{\partial r^*} + \frac{1}{b\sin\theta^*} \frac{\partial \left(\sin\theta^* u_\theta^*\right)}{\partial \theta^*} = 0,\tag{4}$$

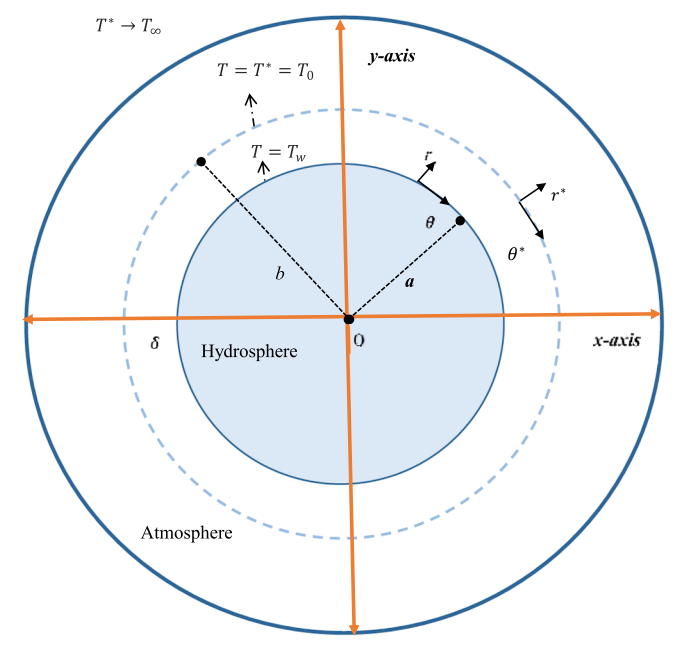


Fig. 1. Schematic Diagram.

$$\rho^* \left(u_r^* \frac{\partial u_\theta^*}{\partial r^*} + \frac{u_\theta^*}{b} \frac{\partial u_\theta^*}{\partial \theta^*} \right) = \frac{\partial}{\partial r^*} \left(\mu^* \frac{\partial u_\theta^*}{\partial r^*} \right) \pm g^* \rho_\infty^* \beta^* (T^* - T_\infty) \cos \gamma^*, \tag{5}$$

$$\rho^* C_p^* \left(u_r^* \frac{\partial T^*}{\partial r^*} + \frac{u_\theta^*}{b} \frac{\partial T^*}{\partial \theta^*} \right) = \frac{\partial}{\partial r^*} \left(k^* \frac{\partial T^*}{\partial r^*} \right), \tag{6}$$

subject to boundary conditions

atr = a

$$u_{\theta} = 0, \ u_{r} = 0, \ T = T_{w},$$
 (7a)

at $r = \delta$ (interface)

$$r^* = b, \quad u_\theta = u_\theta^* = 0, \quad T = T_0, \quad T^* = T_0 + \pi_L \frac{\partial T^*}{\partial r}$$
 (7b)

as $r^* \to \infty$

$$u_q^* \to 0, \quad T^* \to T_\infty$$
 (7c)

where $\pi_L = \sigma_T \lambda$ with σ_T = thermal slip coefficient and λ = average distance travelled by air. As density is supposed temperature dependent for hydrosphere phase while variation in other fluid properties of hydrosphere is neglected in comparison to atmospheric phase. Thus

$$\rho = \rho^* e^{-[\beta(T-T^*)]}$$

$$\rho^* = \rho_{\infty} e^{-[\beta^* (T^* - T_{\infty})]},\tag{8}$$

$$\mu^* \cong \mu_{\infty}^* [1 + \varepsilon^* (T^* - T_{\infty})],$$

and

$$k^* \cong k_\infty^* [1 + \eta^* (T^* - T_\infty)].$$

3. Dimensionless model

Eq. (8) is introduced, and by combining the appropriate variables listed below, the governing equations from Eq. (1-7) are transformed into dimensionless forms:

$$\widehat{r} = \frac{r-a}{a}, \quad \widehat{u}_r = \frac{au_r}{\nu}, \quad \widehat{u}_\theta = \frac{au_\theta}{\nu}, \quad \widehat{\theta} = \theta, \phi = \frac{T-T^*}{T_{\cdots}-T^*}$$

$$\widehat{r}^* = \frac{r^* - b}{b}, \quad \widehat{u}_r^* = \frac{bu_r^*}{\nu^*}, \quad \widehat{u}_\theta^* = \frac{bu_\theta^*}{\nu^*}, \qquad \widehat{\theta}^* = \theta^*, \quad \phi^* = \frac{T^* - T_\infty}{T_0 - T_\infty}, \tag{9}$$

Hydrosphere phase

$$\frac{\partial \widehat{u}_r}{\partial \widehat{r}} + \frac{1}{\sin \widehat{\theta}} \frac{\partial \sin \widehat{\theta} \, \widehat{u}_{\theta}}{\partial \widehat{\theta}} = 0, \tag{10}$$

$$\widehat{u}_{r}\frac{\partial \widehat{u}_{\theta}}{\partial \widehat{r}} + \widehat{u}_{\theta}\frac{\partial \widehat{u}_{\theta}}{\partial \widehat{\theta}} = \frac{\partial}{\partial \widehat{r}} \left(e^{\beta_{H}\phi} \frac{\partial \widehat{u}_{\theta}}{\partial \widehat{r}} \right) \pm Gr_{H}\phi \cos\gamma, \tag{11}$$

$$\widehat{u}_{r}\frac{\partial\phi}{\partial\widehat{r}} + \widehat{u}_{\theta}\frac{\partial\phi}{\partial\theta} = \frac{1}{\Pr_{H}}\frac{\partial}{\partial\widehat{r}}\left(e^{\beta_{H}\phi}\frac{\partial\phi}{\partial\widehat{r}}\right). \tag{12}$$

Atmosphere phase

$$\frac{\partial \widehat{u}_{r}^{*}}{\partial \widehat{r}^{*}} + \frac{1}{\sin \widehat{\theta}^{*}} \frac{\partial \left(\sin \widehat{\theta}^{*} \widehat{u}_{\theta}^{*}\right)}{\partial \widehat{\theta}^{*}} = 0, \tag{13}$$

$$e^{-\beta_A\phi^*}\left(\widehat{u}_r^*\frac{\partial\widehat{u}_\theta^*}{\partial\widehat{r}^*}+\widehat{u}_\theta^*\frac{\partial\widehat{u}_\theta^*}{\partial\widehat{\wp}^*}\right) = \frac{\partial}{\partial\widehat{r}^*}\left((1+\varepsilon_A\phi^*)\frac{\partial\widehat{u}_\theta^*}{\partial\widehat{r}^*}\right) \pm \mathrm{Gr}_A\phi^*\mathrm{cos}\gamma^*, \tag{14}$$

$$e^{-\beta_A\phi^*}\left(\widehat{u}_r^*\frac{\partial\phi^*}{\partial\widehat{r}^*}+\widehat{u}_\theta^*\frac{\partial\phi^*}{\partial\widehat{\theta}^*}\right) = \frac{1}{\Pr_A}\frac{\partial}{\partial\widehat{r}^*}\left(\left(1+\eta_A\phi^*\right)\frac{\partial\phi^*}{\partial\widehat{r}^*}\right),\tag{15}$$

subject to boundary conditions

(5)
$$at\widehat{r} = 0, \quad \widehat{u}_{\theta} = 0, \quad \widehat{u}_{r} = 0, \phi = 1, \\ at\widehat{r} = (\widehat{r})_{\delta}, \qquad \widehat{u}_{\theta} = 0, \phi = 0,$$
 (16a)

$$\begin{array}{ll}
\operatorname{at}\widehat{r}^{*} = 0, & u_{\theta}^{*} = 0, & \phi^{*} = 1 + \omega_{T} \frac{\partial \phi^{*}}{\partial \widehat{r}}, \\
\operatorname{as}\widehat{r}^{*} \to \infty, & u_{\theta}^{*} \to 0, & \phi^{*} \to 0
\end{array} \right\} (\text{for atmosphere phase}) \tag{16b}$$

where ω_T is thermal slip parameter.

$$\begin{split} \Pr_H &= \nu/\alpha \quad, \quad \Pr_A = \nu^*/\alpha^*, \quad \operatorname{Gr}_H = \frac{g\beta(T_w - T^*)\alpha^3}{\upsilon^2}, \quad \operatorname{Gr}_A \\ &= \frac{g^*\beta^*(T_b - T_\infty)b^3}{\upsilon^{*2}} \\ \beta_H &= (T_w - T^*)\beta, \quad \beta_A = (T_b - T_\infty)\beta^*, \quad \varepsilon_A = (T_b - T_\infty)\varepsilon^*, \quad \eta_A = (T_b - T_\infty)\eta^*, \quad \omega_T = \frac{\pi_L}{a} \,. \end{split}$$

4. Methodological framework

We have used the finite difference technique, a well-known approach in computational fluid dynamics and related fields, to study the current topic. The finite difference approach discretizes differential equations, converting them into algebraic equations that may be solved iteratively. We will present the following primitive variable formulation in order to use the previously mentioned procedure.

$$R = \widehat{r}\widehat{\theta}^{-\frac{1}{4}}, \Theta = \widehat{\theta}, \quad \widehat{u}_{\theta} = \widehat{\theta}^{\frac{1}{2}}U_{\theta}, \quad \widehat{u}_{r} = \widehat{\theta}^{-\frac{1}{4}}U_{r}, \Phi = \phi$$

$$R^{*} = \widehat{r}^{*}\widehat{\theta}^{-\frac{1}{4}}, \quad \widehat{u}_{\theta}^{*} = \widehat{\theta}^{\frac{1}{2}}U_{\theta}^{*}, \quad \widehat{u}_{r}^{*} = \widehat{\theta}^{-\frac{1}{4}}U_{r}^{*}, \quad \Phi^{*} = \phi^{*} \quad , \tag{17}$$

It converts Eq. (10-16) into the following appropriate form. Hydrosphere

$$\Theta \frac{\partial U_{\theta}}{\partial \Theta} + \frac{1}{2} U_{\theta} + -\frac{R}{4} \frac{\partial U_{\theta}}{\partial R} + + \Theta U_{\theta} \cot \Theta + \frac{\partial U_{r}}{\partial R} = 0, \tag{18}$$

$$\Theta U_{\theta} \frac{\partial U_{\theta}}{\partial \Theta} + \left[U_r - \frac{R}{4} U_{\theta} \right] \frac{\partial U_{\theta}}{\partial R} + \frac{1}{2} U_{\theta}^2 = \frac{\partial}{\partial R} \left(e^{\theta_H \Phi} \frac{\partial U_{\theta}}{\partial R} \right) + G r_H \Phi \cos \gamma, \tag{19}$$

$$\Theta U_{\theta} \frac{\partial \Phi}{\partial \Theta} + \left[U_r - \frac{R}{4} U_{\theta} \right] \frac{\partial \Phi}{\partial R} = \frac{1}{\Pr_{\theta}} \frac{\partial}{\partial R} \left(e^{\theta_H \Phi} \frac{\partial \Phi}{\partial R} \right). \tag{20}$$

Atmosphere

$$\Theta^* \frac{\partial U^*_{\theta}}{\partial \Theta^*} + \frac{1}{2} U^*_{\theta} + -\frac{R^*}{4} \frac{\partial U^*_{\theta}}{\partial R^*} + +\Theta^* U^*_{\theta} \cot \Theta^* + \frac{\partial U^*_{r}}{\partial R^*} = 0, \tag{21}$$

$$\begin{split} e^{-\beta_{A}\Phi^{*}} \left(\Theta^{*} U_{\theta}^{*} \frac{\partial U_{\theta}^{*}}{\partial \Theta^{*}} + \left[U_{r}^{*} - \frac{R^{*}}{4} U_{\theta}^{*} \right] \frac{\partial U_{\theta}^{*}}{\partial R^{*}} + \frac{1}{2} U_{\theta}^{*2} \right) \\ = \frac{\partial}{\partial R^{*}} \left((1 + \varepsilon_{A} \Phi^{*}) \frac{\partial U_{\theta}^{*}}{\partial R^{*}} \right) + G r_{A} \Phi^{*} \cos \gamma, \end{split} \tag{22}$$

$$e^{-\beta_A \Phi^*} \left(\Theta^* U_{\theta}^* \frac{\partial \Phi^*}{\partial \Theta^*} + \left[U_r^* - \frac{R^*}{4} U_{\theta}^* \right] \frac{\partial \Phi^*}{\partial R^*} \right) = \frac{1}{\Pr_A} \frac{\partial}{\partial R^*} \left((1 + \eta_A \Phi^*) \frac{\partial \Phi^*}{\partial R^*} \right), \tag{23}$$

with transformed boundary conditions

$$\begin{array}{ll} \text{at}R=0, & U_{\theta}=0, & U_{r}=0, \Phi=1\\ \text{at}R=\left(R\right)_{\delta}, & U_{\theta}=0, \Phi=0, \end{array}, \ \left. \right\} (\text{for hydrosphere phase}) \end{array} \tag{24a}$$

$$atR^* = 0, \quad U_{\theta}^* = 0, \quad \Phi^* = 1 + \omega_T \Theta^{\frac{-1}{4}} \frac{\partial \Phi^*}{\partial R},$$
 (for atmosphere phase)
$$asR^* \rightarrow \infty, \qquad U_{\theta}^* \rightarrow 0, \quad \Phi^* \rightarrow 0 \quad .$$
 (24b)

5. Computational strategy

We discretize the domains of R and Θ for the hydrosphere phase and R^* and Θ^* for the atmospheric phase in order to analyze the proposed problem. To approximate the derivatives for each phase, the central difference and backward difference schemes are applied along radial and tangential directions, respectively.

Hydrosphere

$$rac{\partial U_{ heta}}{\partial \Theta} = rac{U_{ heta_{(i,j)}} - U_{ heta_{(i,j-1)}}}{\Delta \Theta},$$

$$\frac{\partial U_{\theta}}{\partial R} = \frac{U_{\theta_{(i+1,j)}} - U_{\theta_{(i-1,j)}}}{2\Delta R},$$

$$\frac{\partial^{2} U_{\theta}}{\partial R^{2}} = \frac{U_{\theta_{(i+1,j)}} - 2U_{\theta_{(i,j)}} + U_{\theta_{(i-1,j)}}}{\Delta R^{2}}.$$
 (25)

Atmosphere

$$\frac{\partial U_{ heta}^*}{\partial \Theta^*} = \frac{U_{ heta_{(i,j)}}^* - U_{ heta_{(i,j-1)}}^*}{\Delta \Theta^*},$$

$$rac{\partial U_{ heta}^*}{\partial R^*} = rac{U_{ heta_{(i+1,j)}}^* - U_{ heta_{(i-1,j)}}^*}{2\Delta R^*},$$

$$\frac{\partial^2 U_{\theta}^*}{\partial R^{*2}} = \frac{U_{\theta_{(i+1,j)}}^* - 2U_{\theta_{(i,j)}}^* + U_{\theta_{(i-1,j)}}^*}{\Delta R^{*2}},\tag{26}$$

where i,j are the grid points along radial and tangential directions with step sizes ΔR , ΔR^* and $\Delta \Theta$, $\Delta \Theta^*$ respectively. Substitution of Eqs. (24)-(25) into Eqs. (17)-(23) yield the following system of equations.

Hydrosphere

$$\begin{split} U_{r_{(i+1j)}} &= U_{r_{(i-1j)}} + \frac{R_j}{4} \left(U_{\theta_{(i+1j)}} - U_{\theta_{(i-1j)}} \right) - \Delta R U_{\theta_{(ij)}} - 2\Delta R \Theta_i U_{\theta_{(ij)}} \cot \Theta_i \\ &\qquad - \frac{2\Delta R \Theta_i}{\Delta \Theta} \left(U_{\theta_{(ij)}} - U_{\theta_{(ij-1)}} \right), \end{split} \tag{26}$$

$$AU_{\theta_{(i-1)}} + BU_{\theta_{(i)}} + CU_{\theta_{(i+1)}} = D, (27)$$

with

$$A = e^{\beta_H \Phi_{(i,j)}} + \frac{\Delta R}{2} \left[U_{r_{(i,j)}} - \frac{R_j}{4} U_{\theta_{(i,j)}} \right] - \frac{\beta_H}{4} e^{\beta_H \Phi_{(i,j)}} \left(\Phi_{(i+1,j)} - \Phi_{(i-1,j)} \right), \tag{27a}$$

$$B=-2e^{ heta_{H}\Phi_{(i,j)}}-\left(rac{\Delta R^{2}}{2}+rac{\Delta R^{2}}{\Delta\Theta}\Theta_{i}
ight)U_{ heta_{(i,j)}}, \eqno(27b)$$

$$C = e^{\theta_H \Phi_{(i,j)}} - \frac{\Delta R}{2} \left[U_{r_{(i,j)}} - \frac{R_j}{4} U_{\theta_{(i,j)}} \right] + \frac{\beta_H}{4} e^{\theta_H \Phi_{(i,j)}} \left(\Phi_{(i+1,j)} - \Phi_{(i-1,j)} \right), \tag{27c}$$

$$D = -\frac{\Delta R^2 \Theta_i}{\Delta \Theta} U_{\theta_{(i,j)}} U_{\theta(i,j-1)} + \Delta R^2 Gr_H \Phi_{(i,j)} \cos\gamma, \tag{27d}$$

and

$$A'\Phi_{\theta(i-1,j)} + B'\Phi_{\theta(i,j)} + C'\Phi_{\theta(i+1,j)} = D',$$
(28)

with

$$A' = \frac{e^{\beta_H \Phi_{(i,j)}}}{\Pr} + \frac{\Delta R}{2} \left[U_{r_{(i,j)}} - \frac{R_j}{4} U_{\theta_{(i,j)}} \right] - \frac{\beta_H}{4} e^{\beta_H \Phi_{(i,j)}} \left(\Phi_{(i+1,j)} - \Phi_{(i-1,j)} \right), \tag{28a}$$

$$B' = -\frac{2e^{\theta_H \Phi_{(i,j)}}}{\text{Pr}} - \frac{\Delta R^2}{\Delta \Theta} \Theta_i U_{\theta_{(i,j)}}, \tag{28b}$$

$$C' = \frac{e^{\beta_H \Phi_{(i,j)}}}{\Pr} - \frac{\Delta R}{2} \left[U_{r_{(i,j)}} - \frac{R_j}{4} U_{\theta_{(i,j)}} \right] + \frac{\beta_H}{4} e^{\beta_H \Phi_{(i,j)}} \left(\Phi_{(i+1,j)} - \Phi_{(i-1,j)} \right), \quad (28c)$$

$$D' = -\frac{\Delta R^2}{\Delta \Theta} \Theta_i U_{\theta_{(ij)}} \Phi_{(ij-1)}, \tag{28d}$$

where A,B and C are coefficients of unknown variables $U_{\theta_{(i-1,j)}},U_{\theta_{(i,j)}}$ and $U_{\theta_{(i+1,j)}}$ and A',B' and C' are coefficients of unknown variables $\Phi_{(i,j-1)},\Phi_{(i,j)}$ and $\Phi_{(i,j+1)}$.

Atmosphere

$$\begin{split} U_{r_{(i+1,j)}}^* &= U_{r_{(i-1,j)}}^* + \frac{R_j^*}{4} \left(U_{\theta_{(i+1,j)}}^* - U_{\theta_{(i-1,j)}}^* \right) - \Delta R^* U_{\theta_{(i,j)}}^* - 2\Delta R^* \Theta_i^* U_{\theta_{(i,j)}}^* \cot \Theta_i^* \\ &- \frac{2\Delta R^* \Theta_i^*}{\Delta \Theta^*} \left(U_{\theta_{(i,j)}}^* - U_{\theta_{(i,j-1)}}^* \right), \end{split}$$

$$A^* U^*_{\theta_{(i-1)i}} + B^* U^*_{\theta_{(i)i}} + C^* U^*_{\theta_{(i+1)i}} = D^*$$
(30)

where

$$A^* = \left(1 + \varepsilon_A \Phi^*_{(i,j)}\right) + \frac{\Delta R^*}{2} e^{-\beta_A \Phi^*_{(i,j)}} \left[U^*_{r_{(i,j)}} - \frac{R_j}{4} U^*_{\theta_{(i,j)}} \right] - \frac{\varepsilon_A}{4} \left[\Phi^*_{(i+1,j)} - \Phi^*_{(i-1,j)} \right], \tag{30a}$$

$$B^* = -2\Big(1 + \varepsilon_A \Phi^*_{(i,j)}\Big) - e^{-eta_A \Phi^*_{(i,j)}} \Big(rac{\Delta R^{*\,2}}{2} + rac{\Delta R^{*\,2}}{\Delta \Theta^*} \Theta_i\Big) U^*_{\theta_{(i,j)}},$$
 (30b)

$$C^* = \left(1 + \varepsilon_A \Phi^*_{(i,j)}\right) - \frac{\Delta R^*}{2} e^{-\beta_A \Phi^*_{(i,j)}} \left[U^*_{r_{(i,j)}} - \frac{R_j}{4} U^*_{\theta_{(i,j)}} \right] + \frac{\varepsilon_A}{4} \left[\Phi^*_{(i+1,j)} - \Phi^*_{(i-1,j)} \right], \tag{30c}$$

$$D^* = \frac{\Delta R^{*2} \Theta_i^*}{\Delta \Theta^*} e^{-\beta_A \Phi_{(i,j)}^*} U_{\theta_{(i,j-1)}}^* + \Delta R^{*2} Gr_A \Phi_{(i+1,j)}^* \cos \gamma^*, \tag{30d}$$

and

$$A^{r^*}\Phi_{\theta(i-1,j)} + B^{r^*}\Phi_{\theta(i,j)} + C^{r^*}\Phi_{\theta(i+1,j)} = D^{r^*},$$
(31)

such that

$$A'^* = \frac{\left(1 + \eta_A \Phi^*_{(i,j)}\right)}{\Pr} + \frac{\Delta R^*}{2} e^{-\beta_A \Phi^*_{(i,j)}} \left[U^*_{r_{(i,j)}} - \frac{R_j}{4} U^*_{\theta_{(i,j)}} \right] - \frac{\eta_A}{4} \left[\Phi^*_{(i+1,j)} - \Phi^*_{(i-1,j)} \right], \tag{31a}$$

$$B^* = -rac{2\Big(1+\eta_A\Phi^*_{(i,j)}\Big)}{\operatorname{Pr}} - e^{-eta_A\Phi^*_{(i,j)}}rac{\Delta R^{*\,2}}{\Delta\Theta^*}\Theta_i U^*_{ heta_{(i,j)}},$$
 (31b)

$$C^* = \frac{\left(1 + \eta_A \Phi^*_{(i,j)}\right)}{\Pr} - \frac{\Delta R^*}{2} e^{-\beta_A \Phi^*_{(i,j)}} \left[U^*_{r_{(i,j)}} - \frac{R_j}{4} U^*_{\theta_{(i,j)}} \right] + \frac{\eta_A}{4} \left[\Phi^*_{(i+1,j)} - \Phi^*_{(i-1,j)} \right], \tag{31c}$$

$$D^{*} = -\frac{\Delta R^{*2} \Theta_{i}^{*}}{\Delta \Theta^{*}} e^{-\beta_{A} \Phi_{(i,j)}^{*}} U_{\theta_{(i,j)}}^{*} \Phi_{(i,j-1)}^{*}, \tag{31d}$$

where A^* , B^* and C^* are coefficients of unknown variables $U^*_{\theta_{(i-1)j}}$, $U^*_{\theta_{(ij)}}$ and $U^*_{\theta_{(i+1)j}}$ and A'^* , B'^* and C^* are coefficients of unknown variables $\Phi^*_{(i-1)j}$, $\Phi^*_{(ij)}$ and $\Phi^*_{(i+1)j}$.

with boundary conditions

$$\begin{array}{ll} \text{at} R_{j} = 0, & U_{\theta_{(i,j)}} = 0, & U_{r_{(i,j)}} = 0, & \Phi_{(i,j)} = 1 \\ \text{at} R_{j} = \left(R_{j}\right)_{\delta}, & U_{\theta_{(i,j)}} = 0, & \Phi_{(i,j)} = 0 \end{array} \right\} (\text{for hydrosphere phase}), \tag{32a}$$

$$\text{at}R_{j}^{*} = 0, U_{\theta_{(i,j)}}^{*} = 0, \quad \Phi_{(i,j)}^{*} = 1 + S_{T}$$

$$\text{as}R_{j}^{*} \rightarrow \infty, \quad U_{\theta_{(i,j)}}^{*} \rightarrow 0, \quad \Phi_{(i,j)}^{*} \rightarrow 0$$

$$\text{(32b)}$$

where
$$S_T = \omega_T \Theta_{-1}^{-1} \frac{\Phi_{(i+1,j)}^* - \Phi_{(i-1,j)}^*}{2AR^*}$$

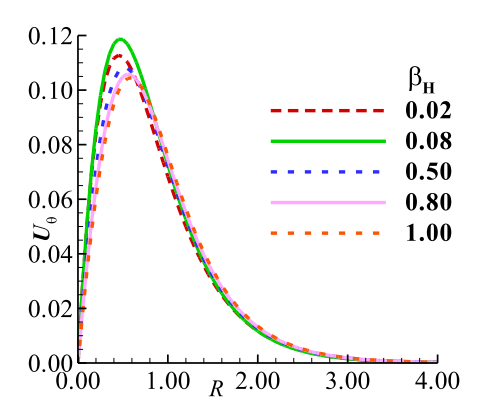
Using FORTRAN Laher-95, the tri-diagonal algebraic Eq. (26–32) are solved for both regions via Gaussian elimination technique. The computation begins at the hydrosphere's surface in the first phase, and at each location under consideration, the effects of temperature and flow are produced normal to the surface. Similar to the first region, the second region's computation began at the atmosphere's surface, and the results are graphically represented for both phases using Tecplot-360.

6. Results and discussion

The impact of variable density of hydrosphere and atmosphere on climate change in atmospheric region by including thermal jump effects in atmosphere is analysed. To explore the impact of variable density of hydrosphere region, Fig. 2a and b, which depict the velocity profile and temperature distribution at $\gamma = 1.5$ radian has been provided with numerous representative values of density variation parameter. It shows that while the temperature distribution rises with increasing values of density variation parameter, the velocity profile is reduced. It can be seen that thermal distribution is maximum for $\beta_H=1.0$, the flow velocity is minimum for $\beta_H=0.02$ at the position $\gamma=1.5$ radian. Density variations in hydrosphere, driven primarily by temperature differences, have deep impacts on climate change, as they effect on ocean heat storage, sea level rise, and weather patterns. These processes are interrelated, forming feedback loops that can accelerate climate change and lead to more extreme weather events, disrupted ecosystems, and causes global warming. Temperature distribution reduces with increasing values of Grashof number Gr_H, however flow speed is increased, as shown in Fig. 3a and b. For $Gr_H = 100$ temperature distribution is minimum and the velocity profile is maximum at the position $\gamma = 1.5$ radian. These findings reveal the direct impact of the Grashof number on the flow regime's temperature and rate of heat transfer. A high Grashof number indicates significant buoyant forces relative to viscous forces in flow, which increases natural convection. Strong convection currents dispersed heat more evenly throughout the fluid, lowering the temperature differences. Fig. 4a and b represent the velocity and thermal profiles with different values of Prandtl number Pr_H. It can be observed that for low value of Prandtl number i.e. for $Pr_H = 3.6$ the velocity profile and temperature distribution are high as compared to large value $Pr_H = 13.7$ at the position $\gamma = 1.5$ radian. For higher Prandtl number the thermal diffusivity reduced and results in more localized heat distribution, slower mixing, and stronger temperature gradients. These factors could increase the occurrence and intensity of extreme weather phenomena.

The effects of the Grashof number (Gr_A) , viscosity variation parameter (\mathcal{E}_A) , thermal conductivity variation parameter (η_A) , thermal slip parameter (S_T) and density variation parameter (β_A) on the velocity distribution U_θ^* and temperature distribution Φ^* at different locations for the atmospheric phase have been studied. Fig. 5a and b illustrate the

impact of Grashof numbers $Gr_A = 1.0$, 5.0 and 8.0 on the velocity and temperature distributions of the atmospheric phase. The values are measured at different positions $\gamma^* = 0.7$, 1.5 and 3.0 in radian, with fixed parameters, $Pr_A = 0.1$, $\beta_A = 0.03$, $\varepsilon_A = 0.5$, $\eta_A = 0.1$, $S_T = 0.2$. The findings indicate that when heat is transferred from a hightemperature region to a low-temperature region in the atmosphere, the temperature distribution is maximum for $Gr_A = 1.0$ at position $\gamma^* =$ 0.70, while the velocity profile is high for $Gr_A = 8.0$ at position $\gamma^* = 3.0$. A rise in the Grashof number signifies an increase in flow velocity and a decrease in thermal distribution, confirming that buoyancy forces are significantly greater than viscous forces and causing strong natural convection. The effects of viscosity variation parameter $\varepsilon_A = 0.1$, 0.5 and 1.0 are shown in Fig. 6a and b, where $\beta_A = 0.1$, $Gr_A = 2.0$, $\eta_A = 0.1$ 0.02, $S_T = 0.20$ and $Pr_A = 0.71$ are fixed parameters. It can be seen that at location $\gamma^* = 0.7$ for $\varepsilon_A = 0.1$, the velocity profile is maximum and temperature distribution is minimum as compare to, the position $\gamma^* =$ 3.0 for $\varepsilon_A = 1.0$. The climate system is not directly affected by the viscosity variation parameter by itself. It was reflected in the Prandtl number on climate change and had an indirect impact on the Earth's atmosphere's fluid dynamics, convection processes, and heat distribution. The impacts of different values of density variation parameter $\beta_{\Lambda} =$ 0.05, 0.20 and 1.0 on temperature and velocity profiles by fixing other parameters, $\mathrm{Pr}_A = 0.8$, $arepsilon_A = 0.05$, $\mathrm{Gr}_A = 1.0$, $\eta_A = 0.01$, $S_T = 0.10$ are depicted in Fig. 7a and b. The velocity profile is low at position $\gamma^* = 0.70$ for $\beta_A = 0.05$, while the thermal distribution is high at $\gamma^* = 3.0$ for $\beta_A = 0.05$ 1.0. The impacts of the thermal conductivity variation factors $\eta_A = 0.05$, 1.50 and 2.50 are displayed in Fig. 8a and b, while the values of remaining parameters $Pr_A = 0.7$, $\varepsilon_A = 0.07$, $Gr_A = 2.0$, $\beta_A = 0.08$, $S_T = 0.09$ remain unchanged. The velocity distribution and thermal distribution are maximum at location $\gamma^* = 3.0$ for $\eta_A = 2.50$. The rate of heat transfer is increased with increase in η_A , Consequently a rise in the upward heat transfer is noted. This can affect temperature gradients, atmospheric stability, cloud formation, precipitation, and storm progression. Fig. 7a and b display the effects of different values of the Prandtl number $Pr_A = 0.3$, 0.7and1.0 with other parameters remain unchanged. The velocity distribution has value at $\gamma^* = 0.70$ for $Pr_A =$ 0.3, further the temperature distribution is also attain its maximum value at $\gamma^* = 0.70$ for $Pr_A = 0.3$. All of the aforementioned factors have a major contribution on buoyancy, fluid movement, and heat transfer, which in return affects atmospheric processes. The efficiency of energy transfer and environment dynamics within Earth's climate system are impacted by such variations. Fig. 10a and b display the velocity profile and thermal profile with respect to the variation in thermal jump parameter S_T . On observing these figures, as the values of S_T increase, the velocity profile graph increases. Similarly, the temperature graph increases as the values of thermal jump parameter increase and obtain maximum value on thermal jump $S_T = 0.07$ at the position $\gamma^* = 3.0$. The significant jump in temperature in atmospheric region introduces



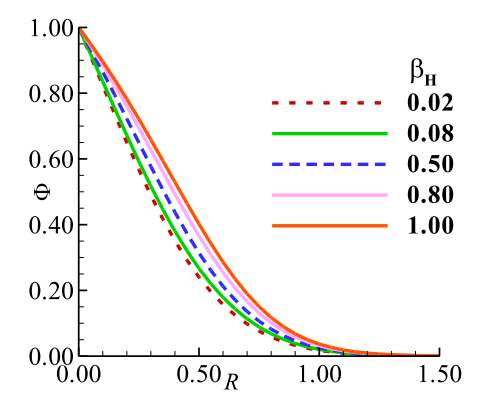


Fig. 2. Analysis of geometrical velocity profile and heat transfer profile for distinct values of density variation parameter β_H = 0.02, 0.08, 0.50 and 1.00, when Pr_H = 5.6, γ = 1.5, and Gr_H = 30 (hydrosphere phase).

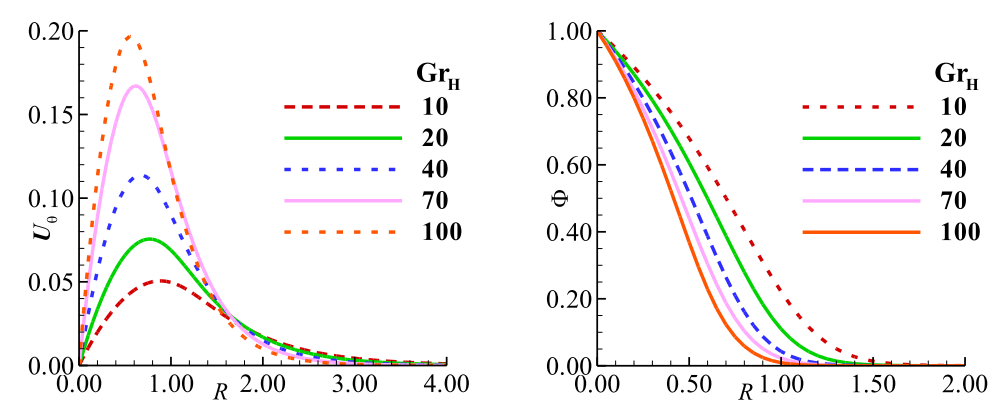


Fig. 3. Analysis of geometrical velocity profile and heat transfer profile for distinct values of Grashof number $Gr_H=10$, 20, 40, 70 and 100, when $Pr_H=7.0$, $\gamma=1.5$ and $\beta_H=2.0$ (hydrosphere phase).

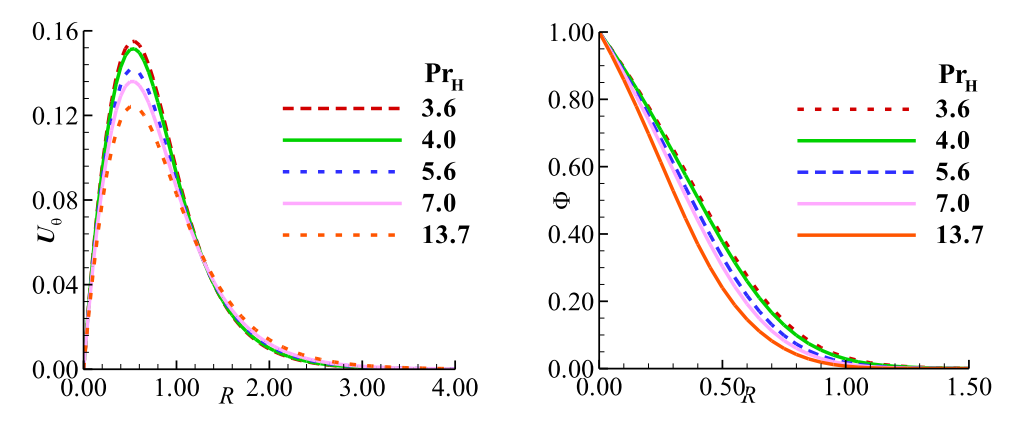


Fig. 4. Analysis of geometrical velocity profile and heat transfer profile for distinct values of Grash of number $Pr_H=3.6, 4.0, 5.6, 7.0$ and 13.7, when $Gr_H=50, \gamma=1.5$ and $\beta_H=1.0$ (hydrosphere phase).

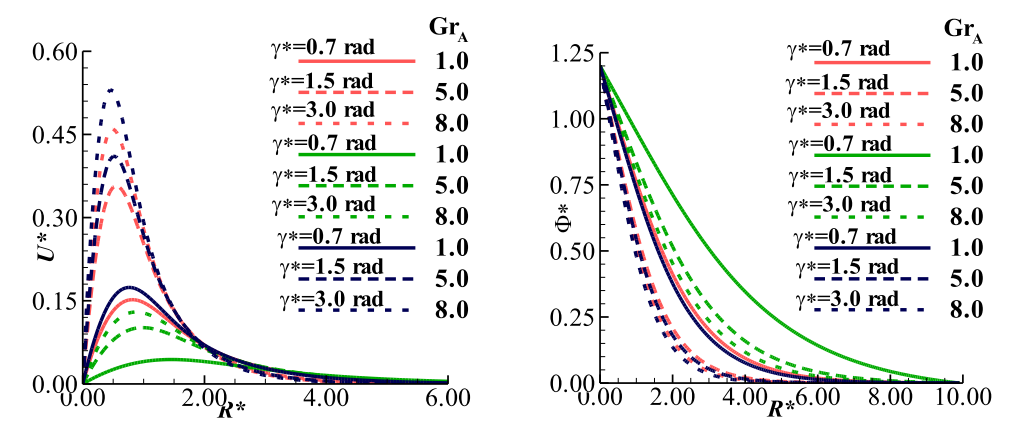


Fig. 5. Analysis of geometrical velocity profile and heat transfer profile for $Gr_A = 1.0, 5.0$ and 8.0 at distinct angles $\gamma^* = 0.7, 1.5$, and 3.14, with $Pr_A = 0.10, \beta_A = 0.03, \epsilon_A = 0.5, \eta_A = 0.10, S_T = 0.2$. (Atmosphere phase).

greater thermal resistance at the boundary which leads to the reduction in overall efficiency of heat transfer. This reduced heat transfer can lead to heat accumulation in the upper layers of the hydrosphere, which might change local temperature dynamics and influence long term climate processes. (Figs. 9–10)

In the atmospheric region flow model, the values of the parameters ${\rm Gr}_A,~~ \epsilon_A,~~ \beta_A,~ \eta_A,~ S_T$ and ${\rm Pr}_A$ at the points $\gamma^*=1.0,~2.5$ and 3.14, measured in radians are displayed in Tables 1, 2, and 3, respectively. These numerical results suggest that at these locations, the heat transfer rate is increased with ${\rm Gr}_A$. The magnitude of heat is accelerated by an increase in the Grashof number in the atmosphere, primarily through

improved buoyancy-driven convection. When the viscosity variation parameter ε_A increases at these locations, the heat transfer rate increases abruptly and then drops. Conduction inside the fluid becomes more important than convection at high value of viscosity variation parameter. Because conduction is frequently slower than convection, the overall rate of heat transfer falls with an increase in values of ε_A . Gradually, the rate at these locations declines after initially increasing with an increase in the density variation parameter β_A . As density increases, the temperature gradient close to the surface is reduced. As thermal variation parameter η_A increases, heat transfer first increases and subsequently declines. The magnitude of the temperature difference

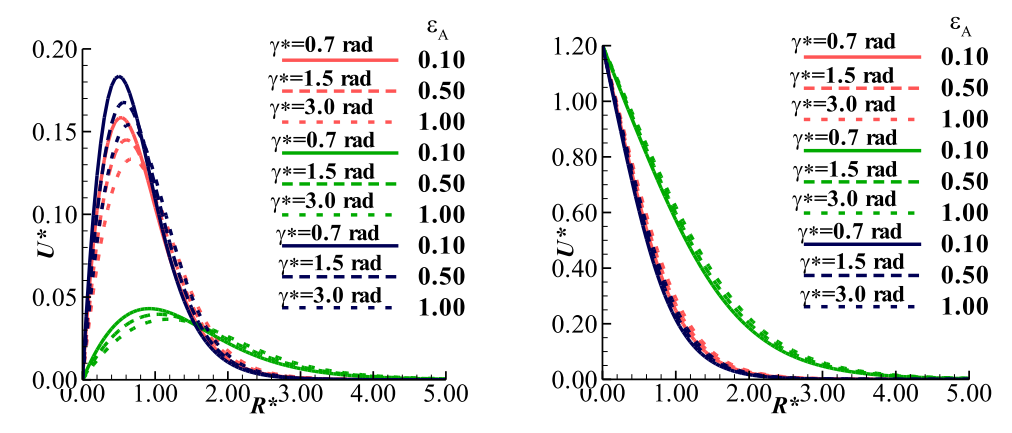


Fig. 6. Analysis of geometrical velocity profile and heat transfer profile for $\varepsilon_A = 0.10$, 0.50 and 1.0 at distinct angles $\gamma^* = 0.7$, 1.5 and 3.0, with $Pr_A = 0.71$, $\beta_A = 0.1$, $Qr_A = 0.0$, $Qr_A = 0.0$, $Qr_A = 0.0$. (Atmosphere phase).

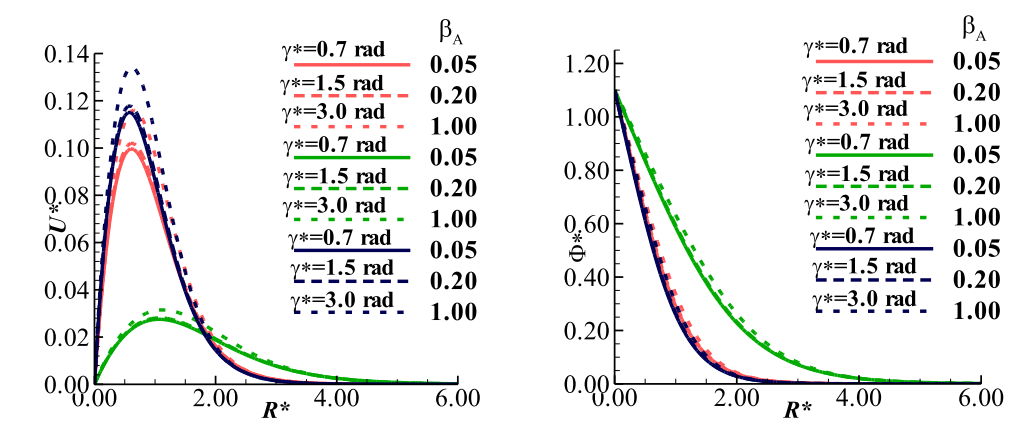


Fig. 7. Geometrical analysis of velocity profile and thermal distribution for $\beta_A=0.05,0.20$ and 1.00 at distinct angles $\gamma^*=0.7,1.5$ and 3.0, with $Pr_A=0.8,\,\varepsilon_A=0.05,\,Gr_A=1.0,\,\eta_A=0.01,\,S_T=0.10.$ (Atmosphere phase).

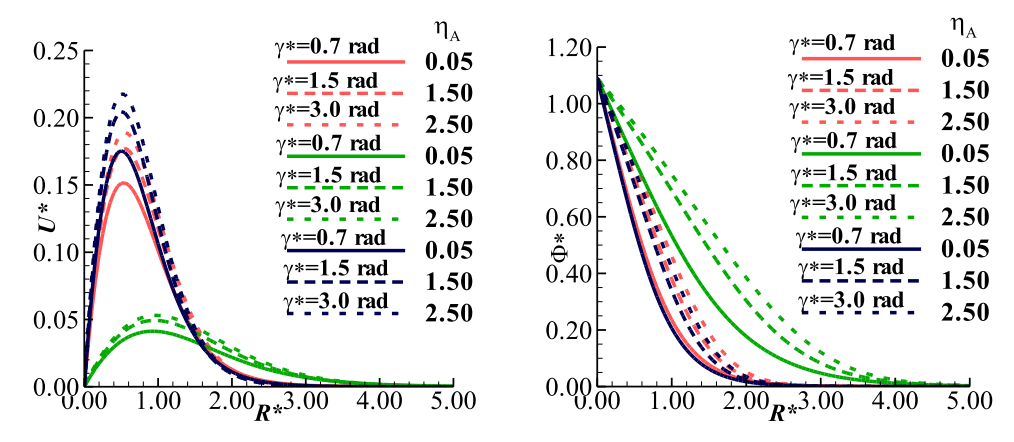


Fig. 8. Geometrical analysis of velocity profile and thermal distribution for $\eta_A=0.05, 1.50$ and 2.50 at distinct angles $\gamma^*=0.7, 1.5$ and 3.0, with $Pr_A=0.7, \epsilon_A=0.07, Gr_A=2, \beta_A=0.08, S_T=0.09$. (Atmosphere phase).

between the hydrosphere and atmosphere grows with an increase in the thermal variation parameter $\eta_A.$ An initial increase in the heat transfer from the warmer to the colder region is caused by this larger gradient, which serves as a stronger driver of heat transfer. The development of a thermocline, a unique layer where the temperature varies quickly with depth can be caused by a strong temperature gradient. When the Prandtl number is greater, heat diffusion proceeds more slowly than momentum diffusion. This facilitates more efficient convective heat transmission since heat is removed from the surface by the moving air. It can be seen

for increasing thermal slip parameter the rate of heat transfer also increases. For the Grashof number $Gr_A=12.0$, the viscosity variation parameter $\varepsilon_A=0.15$, the density variation parameter $\beta_A=0.08$, the thermal conductivity variation parameter $\eta_A=0.08$, $S_T=0.08$ and the Prandtl number $Pr_A=1.0$, the temperature typically reaches its maximum magnitude at position $\gamma^*=3.14$ radian. Concerning the hydrosphere and atmosphere, this suggests that the warm ocean waters can convectively transfer heat to the atmosphere more efficiently at the position $\gamma^*=3.14$ radian. The feedback loops associated with climate

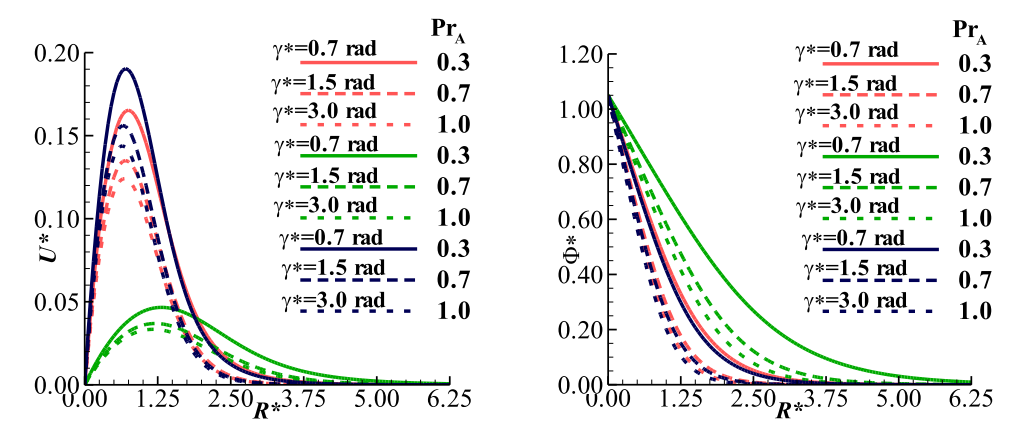


Fig. 9. Geometrical analysis of velocity profile and thermal distribution for $Pr_A = 0.3$, 0.7and1.0 at distinct angles $\gamma^* = 0.7$, 1.5 and 3.0, with $\eta_A = 0.1$, $\varepsilon_A = 1.0$, $Gr_A = 5.0$, $\beta_A = 0.5$, $S_T = 0.05$. (Atmosphere phase).

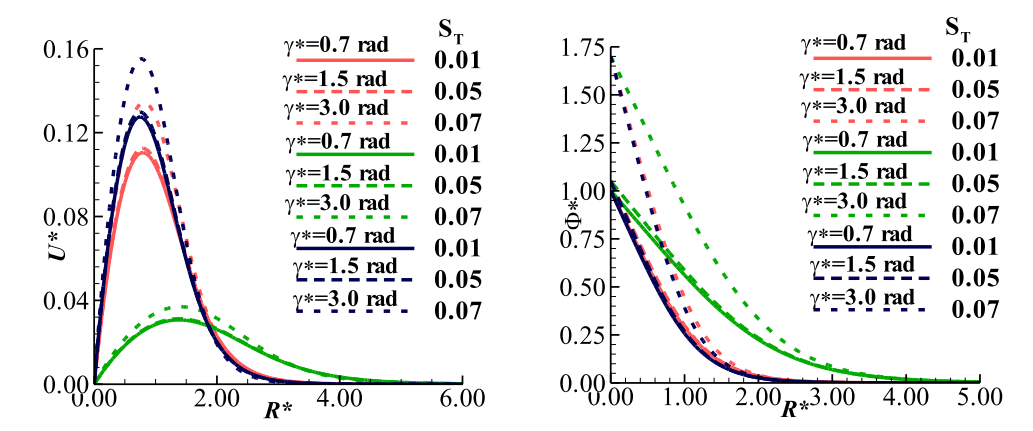


Fig. 10. Geometrical analysis of velocity profile and thermal distribution for $S_T = 0.01$, 0.05, 0.07 at distinct angles $\gamma^* = 0.7$, 1.5 and 3.0, with $\eta_A = 0.1$, $\varepsilon_A = 1.0$, $Gr_A = 2.0$, $\beta_A = 0.5$, $Pr_A = 0.5$. (Atmosphere phase).

change may get worse as a result of this increased heat transfer. Stronger storms and hurricanes can have a greater impact on air circulation and climate patterns because of increased heat convection pattern.

7. Conclusion

The impact of temperature dependent density of hydrosphere and effects of thermal jump condition of atmosphere on climate change has been studied numerically in current study. The effects of variable density in hydrosphere are observed in normal direction. The governing models first transformed into non-dimensional equations in the appropriate format using the primitive variable formulation, and then they are converted into algebraic equations using the finite difference approach. Tecplot-360 is used to graphically display the physical effects of different factors on velocity and thermal profiles. Initially, we have seen how the Grashof number (Gr_H) , Prandtl number (Pr_H) and density variation parameter (β_H) affect the flow profiles and heat distribution for the hydrosphere phase. Likewise, for the dimensionless parameters Grashof number (Gr_A), viscosity variation parameter (ε_A), thermal conductivity variation parameter $(\eta_{A})\text{, Prandtl number }(\text{Pr}_{A})\text{, thermal }$ jump parameter (S_T) and density variation parameter (β_A) , the physical effects on velocity profiles and heat transfer characteristics at different positions due to climate impacts are observed. The effects of thermophysical characteristics on climate change resulting from hydrosphere and atmosphere thermal interaction are summarized below.

 As the values of density variation parameter in hydrosphere region increased, the temperature distribution and velocity profile at position $\gamma^*=1.5$ decreased and increased, respectively. It can be observe from graphical display, velocity profile is minimum for $\beta_H=0.02$ and thermal profile has maximum value for $\beta_H=1.0$ at location $\gamma^*=1.5$

- According to visual representation, with increasing values of Grashof number (Gr_H), the velocity distribution also increases and temperature distribution is deceased in the hydrosphere phase at the position γ* = 1.5.
- The graphical analysis of the velocity and thermal profiles with different values of Prandtl number Pr_H in hydrosphere region shows that for lower value of the Prandtl number $Pr_H = 3.6$ the velocity profile and temperature distribution are high as compared to large value $Pr_H = 13.7$ at position $\gamma^* = 1.5$ radian.
- Graphically, the behavior of the Grashof number (Gr_A) in the atmospheric phase is similar to that in the hydrosphere phase. In the atmospheric phase, the temperature profile has maximum magnitude for $Gr_A = 1.0$ is at $\gamma^* = 0.7$ radian. It indicates that there is more convection at this position, which leads to a uniform temperature distribution. The optimal position to obtain the highest velocity profile value for $Gr_A = 8.0$ is at location $\gamma^* = 3.0$ radian.
- When taking into account the effects of the viscosity variation parameter, it can be seen that the temperature distribution becomes more uniform at location $\gamma^* = 0.7$ for $\varepsilon_A = 0.1$ and the velocity profile rises at position $\gamma^* = 3.0$ radian for $\varepsilon_A = 1.0$.
- The temperature distribution might arise from increased convection, which has been observed when the density variation parameter increases. It is noticed that the velocity profile is low at position γ* = 0.70 radian, while the thermal distribution is high at γ* = 3.0 radian.

Table-1 Heat transfer rate for different values of parameters involved in the flow model in the atmosphere region at position $\gamma^* = 1.0$.

Gr_A	ε_A	β_A	η_A	Pr_A	S_T	Heat Transfer
1.0	-	-	-	-	-	0.31948
5.0	-	-	-	-	-	0.54592
8.0	-	-	-	-	-	0.61922
10.0	-	-	-	-	-	0.65495
12.0	-	-	-	-	-	0.68527
-	0.10	-	-	-	-	0.55646
-	0.15	-	-	-	-	0.62474
-	0.20	-	-	-	-	0.62084
-	0.25	-	-	-	-	0.61710
-	0.30	-	-	-	-	0.61351
-	-	0.05	-	-	-	0.43568
-	-	0.08	-	-	-	0.50707
-	-	0.10	-	-	-	0.50582
-	-	0.15	-	-	-	0.50295
-	-	0.20	-	-	-	0.49999
-	-	-	0.05	-	-	0.47789
-	-	-	0.08	-	-	0.54408
-	-	-	1.00	-	-	0.39001
-	-	-	1.20	-	-	0.36799
-	-	-	1.50	-	-	0.34525
-	-	-	-	0.3	-	0.29915
-	-	-	-	0.5	-	0.39558
-	-	-	-	0.7	-	0.44667
-	-	-	-	0.9	-	0.48690
-	-	-	-	1.0	-	0.50600
-	-	-	-	-	0.01	0.35057
-	-	-	-	-	0.03	0.43857
-	-	-	-	-	0.05	0.44785
-	-	-	-	-	0.07	0.45712
-	-	-	-	-	0.08	0.45712

Table-2 Heat transfer rate for different values of parameters involved in the flow model in the atmosphere region at position $\gamma^* = 2.5$.

Gr_A	ε_A	β_A	η_A	Pr_A	S_T	Heat Transfer
1.0	-	-	-	-	-	0.35199
5.0	-	-	-	-	-	0.60208
8.0	-	-	-	-	-	0.68272
10.0	-	-	-	-	-	0.72218
12.0	-	-	-	-	-	0.75544
-	0.10	-	-	-	-	0.61370
-	0.15	-	-	-	-	0.68871
-	0.20	-	-	-	-	0.68441
-	0.25	-	-	-	-	0.68029
-	0.30	-	-	-	-	0.67634
-	-	0.05	-	-	-	0.48027
-	-	0.08	-	-	-	0.55906
-	-	0.10	-	-	-	0.55768
-	-	0.15	-	-	-	0.55452
-	-	0.20	-	-	-	0.55125
-	-	-	0.05	-	-	0.52697
-	-	-	0.08	-	-	0.59982
-	-	-	1.00	-	-	0.43005
-	-	-	1.20	-	-	0.40576
-	-	-	1.50	-	-	0.38071
-	-	-	-	0.3	-	0.32971
-	-	-	-	0.5	-	0.43615
-	-	-	-	0.7	-	0.49241
-	-	-	-	0.9	-	0.53668
-	-	-	-	1.0	-	0.55770
-	-	-	-	-	0.01	0.38661
-	-	-	-	-	0.03	0.48352
-	-	-	-	-	0.05	0.49375
-	-	-	-	-	0.07	0.50397
-	-	-	-	-	0.08	0.50888

Table-3 Heat transfer rate for different values of parameters involved in the flow model in the atmosphere region at position $\gamma^* = 3.14$.

Gr_A	$arepsilon_A$	β_A	η_A	Pr_A	S_T	Heat Transfer
1.0	-	-	-	-	-	0.41056
5.0	-	-	-	-	-	0.71430
8.0	-	-	-	-	-	0.80934
10.0	-	-	-	-	-	0.85582
12.0	-	-	-	-	-	0.89532
-	0.10	-	-	-	-	0.64688
-	0.15	-	-	-	-	0.72572
-	0.20	-	-	-	-	0.72119
-	0.25	-	-	-	-	0.71687
-	0.30	-	-	-	-	0.71268
-	-	0.05	-	-	-	0.50614
-	-	0.08	-	-	-	0.58914
-	-	0.10	-	-	-	0.58768
-	-	0.15	-	-	-	0.58435
-	-	0.20	-	-	-	0.58091
-	-	-	0.05	-	-	0.55542
-	-	-	0.08	-	-	0.63208
-	-	-	1.00	-	-	0.45322
-	-	-	1.20	-	-	0.42763
-	-	-	1.50	-	-	0.40123
-	-	-	-	0.3	-	0.34745
-	-	-	-	0.5	-	0.45963
-	-	-	-	0.7	-	0.51887
-	-	-	-	0.9	-	0.56547
-	-	-	-	1.0	-	0.58760
-	-	-	-	-	0.01	0.40751
-	-	-	-	-	0.03	0.50953
-	-	-	-	-	0.05	0.52030
-	-	-	-	-	0.07	0.53107
-	-	-	-	-	0.08	0.53624

- For $\eta_A=2.50$, the maximum of the thermal profile and velocity profile is at position $\gamma^*=3.0$. When η_A rises, the rate of heat transfer also rises, meaning that an increase in thermal conductivity variation parameter facilitates upward heat transfer.
- When the impacts of Prandtl number are taken into account, it can be observed that the temperature distribution is more uniform for $Pr_A = 1.0$, while the velocity distribution is uniform for $Pr_A = 0.3$.
- The tabular representation shows that the maximum temperature is at position $\gamma^* = 3.14$ for the Grashof number $Gr_A = 12.0$, the viscosity variation parameter $\varepsilon_A = 0.15$, the density variation parameter $\beta_A = 0.08$, the thermal conductivity variation parameter $\eta_A = 0.08$, thermal jump parameter $S_T = 0.08$ and the Prandtl number $Pr_A = 1.0$.

Further, it is observed that the characteristics of variable density of hydrosphere and thermal inversion in atmosphere affect the climate in different ways when there is thermal interaction between the hydrosphere and atmosphere. Variable density in the hydrosphere can impact the formation and strength of weather phenomena such as hurricanes and monsoons. Additionally, when there is temperature inversion in atmosphere due to thermal jump, it leads to the formation of oceanic layer fog. These inversions can trap pollutants in the neighbor of hydrosphere surface, leading to poor air quality. These effects have significant implications for regional climate patterns, weather systems, and marine ecosystems.

CRediT authorship contribution statement

Iqbal Rabia: Writing – review & editing, Writing – original draft, Visualization, Validation, Software, Investigation, Formal analysis, Data curation, Conceptualization. **Ashraf Muhammad:** Writing – review & editing, Writing – original draft, Visualization, Validation, Supervision,

Software, Resources, Methodology, Investigation, Formal analysis, Data curation, Conceptualization. Rasool Ghulam: Writing – review & editing, Writing – original draft, Visualization, Validation, Supervision, Software, Resources, Project administration, Methodology, Investigation, Funding acquisition, Formal analysis, Data curation, Conceptualization. Alqahtani Ali Saeed: Writing – review & editing, Writing – original draft, Visualization, Validation, Formal analysis, Data curation, Conceptualization. Malik Muhammad Yousaf: Writing – review & editing, Writing – original draft, Visualization, Resources, Funding acquisition, Formal analysis, Data curation, Conceptualization. Chamkha Ali J.: Writing – review & editing, Writing – original draft, Visualization, Resources, Formal analysis, Conceptualization.

Declaration of Competing Interest

The authors declare that they have no known competing financial interests or personal relationships that could have appeared to influence the work reported in this paper.

Acknowledgment

The authors extend their appreciation to the Deanship of Scientific Research at King Khalid University for funding this work through Large Groups Project under grant number RGP. 2/75/1445.

References

- J.C.Y. Koh, E.M. Sparrow, J.P. Hartnett, The two phase boundary layer in laminar film condensation, Int. J. Heat. Mass Transf. 2 (1-2) (1961) 69–82.
- [2] W.H.H. Banks, The boundary layer on a rotating sphere, Q. J. Mech. Appl. Math. 18 (4) (1965) 443–454.
- [3] L.R. Mack, H.C. Hardee, Natural convection between concentric spheres at low Rayleigh numbers, Int. J. Heat. Mass Transf. 11 (3) (1968) 387–396.
- [4] J.A. Scanlan, E.H. Bishop, R.E. Powe, Natural convection heat transfer between concentric spheres, Int. J. Heat. Mass Transf. 13 (12) (1970) 1857–1872.
- [5] J.P. Caltagirone, M. Combarnous, A. Mojtabi, Natural convection between two concentric spheres: transition toward a multicellular flow, Numer. Heat. Transf. 3 (1) (1980) 107–114.
- [6] C. Hsin-Sen, L. Tzong-Shing, Transient natural convection heat transfer between concentric spheres, Int. J. Heat. Mass Transf. 36 (13) (1993) 3159–3170.
- [7] P.J. Webster, The role of hydrological processes in ocean-atmosphere interactions, Rev. Geophys. 32 (4) (1994) 427–476.
- [8] R. Verzicco, P. Orlandi, A finite-difference scheme for three-dimensional incompressible flows in cylindrical coordinates, J. Comput. Phys. 123 (2) (1996) 402–414
- [9] J.M. Khodadadi, Y. Zhang, Effects of buoyancy-driven convection on melting within spherical containers, Int. J. Heat. Mass Transf. 44 (8) (2001) 1605–1618.
- [10] K. Bhattacharyya, S. Mukhopadhyay, G.C. Layek, Steady boundary layer slip flow and heat transfer over a flat porous plate embedded in a porous media, J. Pet. Sci. Eng. 78 (2) (2011) 304–309.
- [11] M.A. Sheremet, Mathematical simulation of unsteady natural convection inside a sphere, Comput. Therm. Sci. Int. J. 3 (4) (2011).

- [12] W. Ibrahim, B. Shankar, MHD boundary layer flow and heat transfer of a nanofluid past a permeable stretching sheet with velocity, thermal and solutal slip boundary conditions, Comput. Fluids 75 (2013) 1–10.
- [13] A.R. Archibold, M.M. Rahman, D.Y. Goswami, E.K. Stefanakos, Analysis of heat transfer and fluid flow during melting inside a spherical container for thermal energy storage, Appl. Therm. Eng. 64 (1-2) (2014) 396–407.
- [14] G. Singh, O.D. Makinde, Mixed convection slip flow with temperature jump along a moving plate in presence of free stream, Therm. Sci. 19 (1) (2015) 119–128.
- [15] V. Ramachandra Prasad, S. Abdul Gaffar, O. Anwar Beg, Free convection flow and heat transfer of tangent hyperbolic past a vertical porous plate with partial slip, J. Appl. Fluid Mech. 9 (4) (2016) 1667–1678.
- [16] S. Siddiqa, M.A. Hossain, R.S.R. Gorla, Temperature-dependent density effect on natural convection flow over a horizontal circular disk, J. Thermophys. Heat. Transf. 30 (4) (2016) 890–896.
- [17] M.I. Khan, M. Tamoor, T. Hayat, A. Alsaedi, MHD boundary layer thermal slip flow by nonlinearly stretching cylinder with suction/blowing and radiation, Results Phys. 7 (2017) 1207–1211.
- [18] J.M. Armengol, F.C. Bannwart, J. Xamán, R.G. Santos, Effects of variable air properties on transient natural convection for large temperature differences, Int. J. Therm. Sci. 120 (2017) 63–79.
- [19] M. Hamid, T. Zubair, M. Usman, Z.H. Khan, W. Wang, Natural convection effects on heat and mass transfer of slip flow of time-dependent Prandtl fluid, J. Comput. Des. Eng. 6 (4) (2019) 584–592.
- [20] Z. Ullah, M. Ashraf, S. Zia, I. Ali, Surface temperature and free-stream velocity oscillation effects on mixed convention slip flow from surface of a horizontal circular cylinder, Therm. Sci. 24 (. 1) (2020) 13–23.
- [21] M. Ashraf, Z. Ullah, Effects of variable density on oscillatory flow around a nonconducting horizontal circular cylinder, AIP Adv. 10 (1) (2020).
- [22] U. Ahmad, M. Ashraf, A. Al-Zubaidi, A. Ali, S. Saleem, Effects of temperature dependent viscosity and thermal conductivity on natural convection flow along a curved surface in the presence of exothermic catalytic chemical reaction, PLoS One 16 (7) (2021) e0252485.
- [23] M. Ashraf, A. Abbas, H.F. Oztop, K.S. Nisar, I. Khan, Computations of mixed convection slip flow around the surface of a sphere: effects of thermophoretic transportation and viscous dissipation, Heat. Transf. 50 (7) (2021) 7349–7362.
- [24] Z. Ullah, M. Ashraf, S. Ahmad, The analysis of amplitude and phase angle of periodic mixed convective fluid flow across a non-conducting horizontal circular cylinder, Partial Differ. Equ. Appl. Math. 5 (2022) 100258.
- [25] A. Abbas, A. Noreen, M.A. Ali, M. Ashraf, E. Alzahrani, R. Marzouki, M. Goodarzi, Solar radiation over a roof in the presence of temperature-dependent thermal conductivity of a Casson flow for energy saving in buildings, Sustain. Energy Technol. Assess. 53 (2022) 102606.
- [26] K.A.M. Alharbi, Z. Ullah, N. Jabeen, M. Ashraf, Magnetohydrodynamic and thermal performance of electrically conducting fluid along the symmetrical and vertical magnetic plate with thermal slip and velocity slip effects, Symmetry 15 (6) (2023) 1148.
- [27] S. Sridhar, M. Muthtamilselvan, Exploring stability of Jeffrey fluids in anisotropic porous media: incorporating Soret effects and microbial systems, Int. J. Numer. Methods Heat. Fluid Flow. (2024).
- [28] M. Saraswathy, D. Prakash, M. Muthtamilselvan, Q.M. Al-Mdallal, Theoretical study on bio-convection of micropolar fluid with an exploration of Cattaneo-Christov heat flux theory, Int. J. Mod. Phys. B 38 (02) (2024) 2450016.
- [29] G.B. Abdelaziz, M. Abdelgaleel, Z.M. Omara, A.S. Abdullah, E.M. El-Said, S. W. Sharshir, A.M. Elsaid, M.A. Dahab, A simplified model of low Re, immiscible, gas-liquid flow, and heat transfer in porous media numerical solution with experimental validation, Exp. Heat. Transf. 37 (2) (2024) 208–231.
- [30] H. Nadeem, M. Ashraf, G. Rasool, S. Tao, Impacts of fossil fuel thermophoretic convective heat transfer on climate change with variable viscosity and thermal conductivity, Phys. Fluids 36 (9) (2024).